Soils and Foundations 2012;52(3):449–464

The Japanese Geotechnical Society

Soils and Foundations

www.sciencedirect.com
journal homepage: www.elsevier.com/locate/sandf

Long-term consolidation behavior interpreted with isotache concept for worldwide clays

Yoichi Watabe[a,*], Kaoru Udaka[b], Yukio Nakatani[c], Serge Leroueil[d]

[a]Leader of Soil Mechanics and Geo-environment Group, Port and Airport Research Institute, 3-1-1, Nagase, Yokosuka 239-0826, Japan
[b]OYO Corporation, 2-61-5, Toro-cho, Kita-ku, Saitama 331-8688, Japan
[c]New Kansai International Airport Co., Ltd., 1, Senshu-Kuko-Kita, Izumisano 549-0001, Japan
[d]Laval University, Québec, Canada G1V 0A6

Available online 11 July 2012

Abstract

The consolidation characteristics interpreted with the isotache concept have been studied by many researchers, including the authors. The aim of most of these studies has been to calculate secondary consolidation with high accuracy in order to evaluate the long-term settlement of large-scale structures. In a previous study, the long-term consolidation characteristics of Osaka Bay clay, collected from the construction site of the Kansai International Airport, were examined, and a simplified method based on the isotache concept, using a compression curve and the relationship between the consolidation yield stress (preconsolidation pressure) and the strain rate, was proposed. The former and the latter were obtained from constant rate of strain consolidation (CRS) tests and long-term consolidation (LT) tests, respectively. The latter is expressed by an equation with three isotache parameters. In addition, it is noteworthy that the isotache parameters can be commonly determined for the Osaka Bay clays retrieved from various depths up to 300 m below the seabed. In the present study, the proposed method was applied to worldwide clays with various characteristics using the common values for the isotache parameters determined for the Osaka Bay clays. It was found that the long-term consolidation behavior of those worldwide clays can be well characterized by the proposed method, along with the common values for the isotache parameters.

Keywords: Long-term consolidation; Secondary consolidation; Isotache; Strain rate; Clay (D05)

1. Introduction

The consolidation characteristics of clay, interpreted with the isotache concept in which the effect of the strain rate on the compression characteristics is considered, have been studied by many researchers, including the authors. The aim of most of these studies has been to calculate secondary consolidation in consideration of the strain rate effect (e.g., Leroueil et al., 1985; Yin et al., 1994; Adachi et al., 1996; Hinchberger and Rowe, 1998; Rowe and Hinchberger, 1998; Kim and Leroueil, 2001; Den Haan and Kamao, 2003; Imai et al., 2005; Tanaka et al., 2006; Watabe et al., 2008; Qu et al., 2010; Degago et al., 2011).

There are three main approaches for the practical and the theoretical evaluations of the consolidation settlement, and these can be listed as follows:

(i) the coupling of Terzaghi's one-dimensional consolidation theory and the constant $C_{\alpha e}$ concept,
(ii) the end of the primary consolidation (EOP) concept (Mesri and Choi, 1985) and the constant $C_{\alpha e}/C_c$ concept

*Corresponding author.
E-mail address: watabe@ipc.pari.go.jp (Y. Watabe).
Peer review under responsibility of The Japanese Geotechnical Society.

Production and hosting by Elsevier

0038-0806 © 2012 The Japanese Geotechnical Society. Production and hosting by Elsevier B.V. All rights reserved.
http://dx.doi.org/10.1016/j.sandf.2012.05.005

Nomenclature

c_1, c_2	constants for Eq. (4)
$C_{\alpha e}$	coefficient of secondary consolidation
$C_{\alpha\varepsilon}$	secondary consolidation index in strain
C_c	compression index
e_0	initial void ratio
p'	vertical effective consolidation pressure (σ'_v)
p'_c	consolidation yield stress (preconsolidation pressure σ'_p)
p'_{c0}	p'_c corresponding to $\dot{\varepsilon}_{vp}=1.0\times10^{-7}\,s^{-1}$
p'_{cL}	the lower limit of p'_c
t	elapsed time
u	pore water pressure
α	slope of $\log p'_c$–$\log\dot{\varepsilon}_{vp}$ relationship ($=C_{\alpha e}/C_c$)
Δu	excess pore water pressure
ε	the total strain
$\dot{\varepsilon}$	total strain rate
ε_0	strain at $p'=\sigma'_{v0}$
ε_e	elastic strain
$\dot{\varepsilon}_{EOP}$	strain rate at the *in situ* end of primary consolidation
ε_{vp}	visco-plastic strain
$\dot{\varepsilon}_{vp}$	visco-plastic strain rate
σ'_{v0}	overburden effective stress

(Mesri and Castro, 1987),
(iii) the isotache concept (Šuklje, 1957)

where $C_{\alpha e}$ is the coefficient of secondary consolidation and C_c is the compression index.

The isotache concept was proposed by Šuklje (1957), who introduced a unique relationship between the strain and the consolidation pressure corresponding to the strain rate in association with viscosity. This concept, which focuses on the strain rate effect, has attracted a lot of attention in recent research works on consolidation. The isotache concept was proposed more than 50 years ago; however, it continues to be studied in academia. Recently, the authors (Watabe et al., 2008) proposed a simplified method with the isotache concept using a reference compression curve and a function of the strain-rate dependency of the consolidation yield stress (preconsolidation pressure) obtained from both constant rate of strain one-dimensional consolidation (CRS) tests and long-term consolidation (LT) tests under a constant applied stress. It is noteworthy that the isotache parameters used in this method can be commonly determined for the Osaka Bay clays retrieved from various depths up to 300 m below the seabed at the Kansai International Airport. This indicates that the method can be very useful in practice, because it is not necessary to determine the parameters at each depth. In this study, we apply the proposed method to the long-term consolidation of not only Osaka Bay clays, but also worldwide clays with various characteristics. Then, we discuss the integrated interpretation of the isotache concept for all of the clays. We also discuss the practical usability of the integrated interpretation.

2. Isotache concept and proposed method

Šuklje (1957) presented a set of isotache behaviors obtained from a series of incremental loading oedometer tests for a lacustrine chalk sample, showing a unique relationship between the strain and the consolidation pressure corresponding to the strain rate in association with the viscosity. Since then, as mentioned above, many research works have focused on the isotache concept in which the effect of the strain rate on the compression characteristics is considered. Leroueil (2006) summarized the recent accumulation of studies related to the isotache concept, and pointed out that slope α of the relationship between the logarithm of the consolidation yield stress (preconsolidation pressure) and the logarithm of the strain rate, which is equal to $C_{\alpha\varepsilon}/C_c$, is essentially a constant in the range of strain rates observed in the laboratory. However, it is probably not constant, but decreases with a decrease in the strain rate in the field, i.e., in the range of small strain rates.

The authors use the very simple equations proposed by Leroueil et al. (1985), but apply them only to the visco-plastic deformation. For clarity, we employ the ε_{vp}–$\log p'$ relationship, where ε_{vp} is the visco-plastic strain, which is defined as the difference between total strain ε, obtained from the consolidation tests, and elastic strain ε_e. We then use the following equations:

$$\varepsilon_{vp}=\varepsilon-\varepsilon_e \tag{1}$$

$$\frac{p'}{p'_c}=f(\varepsilon_{vp}) \tag{2}$$

$$p'_c=g(\dot{\varepsilon}_{vp}) \tag{3}$$

Here p' is the vertical effective consolidation pressure (σ'_v), p'_c is the consolidation yield stress (preconsolidation pressure σ'_p), and $\dot{\varepsilon}_{vp}$ is the strain rate defined as $d\varepsilon_{vp}/dt$. In order to obtain the relationships expressed by Eqs. (2) and (3), CRS and LT tests must be performed. Details will be given later.

Parameter ε_e is defined as the strain expressed by the straight line passing through points (p', ε)=(1 kPa, 0) and (σ'_{v0}, ε_0) on the ε–$\log p'$ curve, as illustrated in Fig. 1(a). Here σ'_{v0} denotes the overburden effective stress and ε_0 denotes the strain at $p'=\sigma'_{v0}$. From the ε–$\log p'$ curve obtained from the CRS tests, ε_{vp} is calculated as the difference between ε and ε_e; the ε_{vp}–$\log p'$ curve is then obtained. Parameter p' is normalized by the value of the consolidation yield stress (preconsolidation pressure), p'_c, read from the ε_{vp}–$\log p'$ curve; and subsequently, the ε_{vp}–$\log p'/p'_c$ curve that corresponds to Eq. (2) is obtained

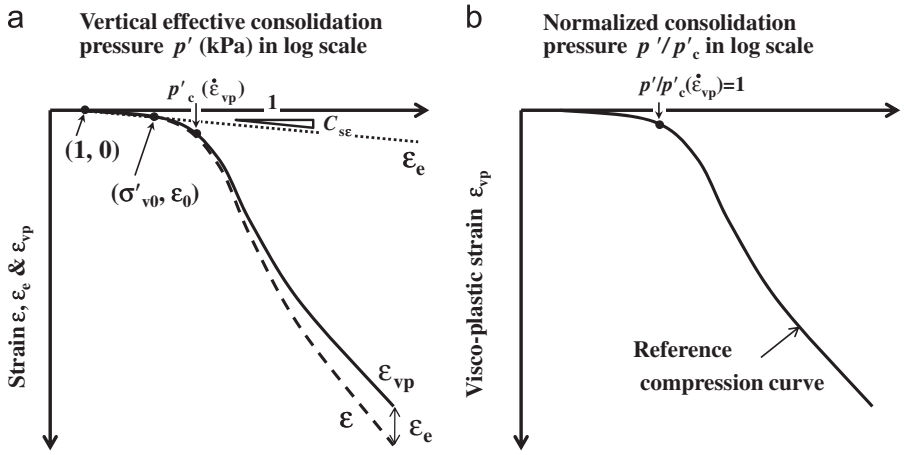

Fig. 1. Compression curve (ε–log p' curve): (a) definition of ε_e and ε_{vp} and (b) reference compression curve.

(Fig. 1(b)). Hereafter, this curve is called the "reference compression curve."

Since pore water pressure u is generally not measured in LT tests, effective consolidation pressure p' cannot be evaluated during primary consolidation. However, during the secondary consolidation stage, the excess pore water pressure is essentially zero ($\Delta u=0$), i.e., p' is equivalent to a p value that is constant. Therefore, $\dot{\varepsilon}$ essentially coincides with $\dot{\varepsilon}_{vp}$.

Parameter $\dot{\varepsilon}_{vp}$ is calculated from the secondary consolidation section (after the end of the primary consolidation: EOP) of the ε–log t curve (consolidation curve) observed in the LT tests under a constant consolidation pressure of p'; $\dot{\varepsilon}_{vp}$ is then obtained as a function of ε_{vp}. The quantity p'/p'_c is obtained as a function of ε_{vp} from the reference compression curve (ε_{vp}–log p'/p'_c curve); $p'_c(\dot{\varepsilon}_{vp})$ is then calculated from p' and $p'/p'_c(\dot{\varepsilon}_{vp})$. This procedure is repeated for some $\dot{\varepsilon}_{vp}$ values, and then the (p'_c, $\dot{\varepsilon}_{vp}$) data set that corresponds to Eq. (3) is obtained.

The model equation for the strain-rate dependency used in this proposed method, i.e., the p'_c–$\dot{\varepsilon}_{vp}$ relationship in Eq. (3), is as follows. Watabe et al. (2008) proposed

$$\ln\frac{p'_c-p'_{cL}}{p'_{cL}}=c_1+c_2\ln\dot{\varepsilon}_{vp} \tag{4}$$

Here c_1 and c_2 are constants and p'_{cL} is the lower limit of p'_c. When $\dot{\varepsilon}_{vp}$ decreases towards zero in Eq. (4), p'_c converges towards p'_{cL}. This equation is consistent with Leroueil (2006) in which it was emphasized that slope α, which is defined as $\Delta\log p'_c/\Delta\log\dot{\varepsilon}_{vp}$, decreases when $\dot{\varepsilon}_{vp}$ decreases to a very small value. Note here that Eq. (4) is essentially the same as that proposed by Qu et al. (2010), in which it was directly derived from Norton's power law (Norton, 1929) in conjunction with the overstress visco-plastic theory (Perzyna, 1963).

Parameter c_1 is equal to $\ln\{(p'_c-p'_{cL})/p'_{cL}\}$ at $\dot{\varepsilon}_{vp}=1$, i.e., it represents the relative position of the $\log p'_c$–$\log\dot{\varepsilon}_{vp}$ curve. Parameter c_2 represents the level of strain-rate dependency. The compressibility of the soil, which reflects the level of the developed skeletal structure, is represented by the reference compression curve expressed by Eq. (2). Consequently, the reference compression curve and the three isotache parameters (p'_{cL}, c_1, and c_2) are required in the proposed method. In the relationship expressed by Eq. (4), if it is assumed that the curve passes a certain point, parameter c_2 is automatically calculated as a dependent variable of p'_{cL} and c_1 (or parameter c_1 is automatically calculated as a dependent variable of p'_{cL} and c_2). Details will be given later.

3. Testing procedure

3.1. Constant rate of strain consolidation tests (CRS tests)

CRS tests were conducted on specimens with a diameter of 60 mm and a height of 20 mm. The cell was filled with de-aired water, and a hydraulic pressure of 98 or 196 kPa was applied as backpressure. The specimen was compressed at a constant $\dot{\varepsilon}_{vp}$ of 0.02%/min ($=3.3\times10^{-6}\,s^{-1}$).

3.2. Long-term consolidation tests (LT tests)

An oedometer was assembled with a specimen having a diameter of 60 mm and a height of 20 mm. A consolidation pressure equivalent to σ'_{v0} was applied for 24 h or seven days. Subsequently, a target pressure was applied for the long-term consolidation until $\dot{\varepsilon}_{vp}$ decreased to $3.3\times10^{-9}\,s^{-1}$. In most cases, it took 30–100 days for the long-term consolidation. Target pressures of σ'_{v0} in the range of 1.5–3.5 times p'_c were specified for each sample. Test conditions will be described later.

4. Compressibility of Osaka Bay clays

4.1. Clay samples

The Osaka Bay clay samples were retrieved from geotechnical investigation sites of the second-phase project of the Kansai International Airport, in Osaka Bay, Japan (Furudoi, 2010). A stratigraphic model of the site is

illustrated in Fig. 2. Here, Ma, Doc, and Ds denote marine clay, lacustrine clay, and diluvial sand. The surface layer, approximately 20 m in thickness, is composed of Holocene clay called Ma13, a very soft non-microstructured clay under normal consolidation. Below this layer is a very thick layer of Pleistocene deposits that are comprised of alternating clay and sand layers. The marine clays are numbered starting from Ma13 and decreasing with depth.

In this study, undisturbed marine clay samples, Ma13, Ma12, Ma11, Ma10, Ma9, Ma8, Ma7, Ma4, and Ma3, are considered. The reconstituted Ma13, which was remolded and preliminarily consolidated under 98 kPa and named Ma13Re, was also tested. The data for Ma13, Ma12, Ma11, Ma8, Ma7, Ma4, and Ma13Re have already been presented in Watabe et al. (2008). The data for Ma10 and Ma9 have been added in this study. The data for Ma7 at different depths (previous Ma7 has been renamed Ma7a, while the new Ma7 has been named Ma7b) and Ma3 are newly obtained. The physical properties of the clay samples are listed in Table 1.

Recently, it was revealed that Ma8 and Ma7 should be renamed Ma7 and Ma6, respectively, because Ma8 was identified in a part of Doc5. However, the original names, which are consistent with the previous studies, are maintained in this study to avoid confusion.

4.2. Test results

All the reference compression curves are shown in Fig. 3. The curve for Ma13Re shows a bi-linear relationship pattern, which yields at p'_c. This pattern is typically observed for non-structured clays. The Ma13 curve is also similar to this. A unique reference curve is formed by the Ma12 to Ma3 curves, and it exhibits overshooting around p'_c and a concave shape in the normal consolidation range, which is usual in micro-structured natural clays.

The test conditions for the LT tests are listed in Table 2. Since most of the data have already been shown in Watabe et al. (2008), only the data sets for Ma10, Ma9, Ma7b, and Ma3, which are newly obtained in this study, are shown

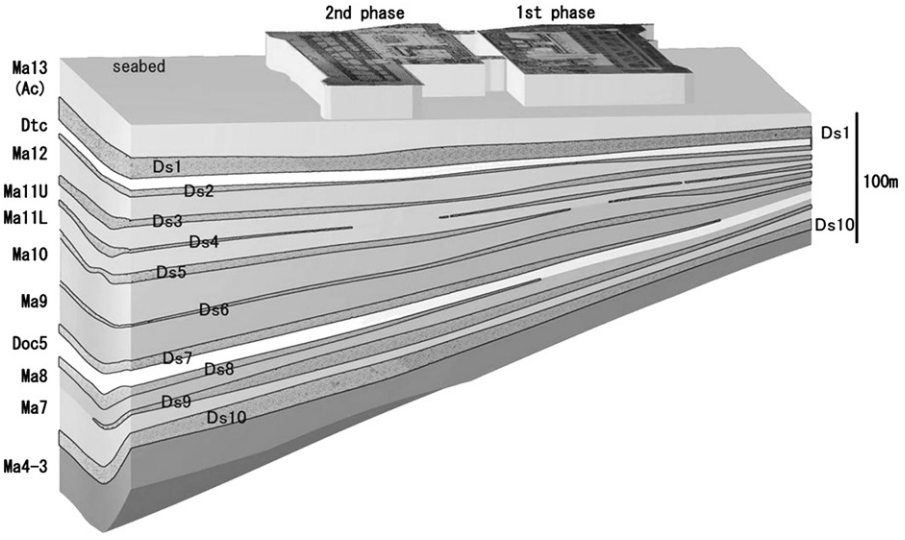

Fig. 2. Stratigraphic model in the cross-shore direction at Kansai International Airport.

Table 1
Physical properties of the Osaka Bay clay samples.

Layer	Ma13	Ma12	Ma11	Ma10	Ma9	Ma8	Ma7a	Ma7b	Ma3	Ma4	Ma13Re
Undisturbed	Yes	Yes	Yes	Yes	Yes	Yes	Yes	Yes	Yes	Yes	No
Reconstituted	No	No	No	No	No	No	No	No	No	No	Yes
Depth (C.D.–m)	39	61	109	161	195	208	223	271	325	264	30–40
Overburden effective stress, σ'_{v0} (kPa)	88	286	619	1014	1262	1348	1457	1839	2278	1802	98
Consolidation yield stress, p'_c (kPa)	122	439	737	1357	1719	1698	1887	1991	3016	2512	134
Overconsolidation ratio, OCR	1.4	1.5	1.2	1.3	1.4	1.3	1.3	1.1	1.3	1.4	1.4
Soil particle density, ρ_s (g/cm^3)	2.66	2.66	2.67	2.69	2.72	2.72	2.70	2.71	2.61	2.67	2.70
Liquid limit, w_L (%)	75	103	89	95	88	92	100	97	119	94	91
Plastic limit, w_P (%)	32	41	34	36	33	36	38	39	42	35	30
Plasticity index, I_p	43	62	55	59	54	56	63	58	77	59	61
Natural water content, w_n (%)	62	84	55	53	52	50	49	53	52	51	72
Natural void ratio, e_n	1.6	2.2	1.5	1.4	1.4	1.4	1.3	1.4	1.4	1.4	1.9

herein. The consolidation curves (ε–log t curves) obtained from the LT tests are shown in Fig. 4. Parameter ε is calculated using the initial specimen height (=20 mm) and it is offset by the strain obtained when the preliminary consolidation under σ'_{v0} was completed. Thus, all the consolidation curves start from a strain of zero.

The long-term consolidation pressure is in the normal consolidation range for all the cases shown here (Ma10, Ma9, Ma7b, and Ma3). Secondary consolidation appears after the end of primary consolidation (EOP). Here, EOP was defined as the point where the strain corresponds to 1.11 (=10/9) times the strain with a 90% degree of consolidation evaluated by the square root t method. The shape of the curves in the secondary consolidation stage is concave, indicating that slope $\Delta\varepsilon_{vp}/\Delta\log t$, which is named the secondary consolidation index in strain ($C_{\alpha\varepsilon}$), gradually decreases with the logarithm of time. The EOP appears after the inflection point between the convex and the concave parts of the curve. Strain rates $\dot{\varepsilon}_{vp}$ along the curves were calculated as $\Delta\varepsilon_{vp}/\Delta t$, and the points corresponding to the $\dot{\varepsilon}_{vp}$ values of 3.3×10^{-5}, 3.3×10^{-6}, 3.3×10^{-7}, 3.3×10^{-8}, and $3.3\times10^{-9}\,s^{-1}$ are shown (markers) on the curves. The relationships between consolidation pressure p', i.e., the long-term consolidation pressure, and ε_{vp} corresponding to these $\dot{\varepsilon}_{vp}$ values, are plotted in Fig. 5 for the Ma10 clay. We can clearly identify the compression line in the normal consolidation range corresponding to each strain rate. This strain-rate dependency is consistent with the isotache concept.

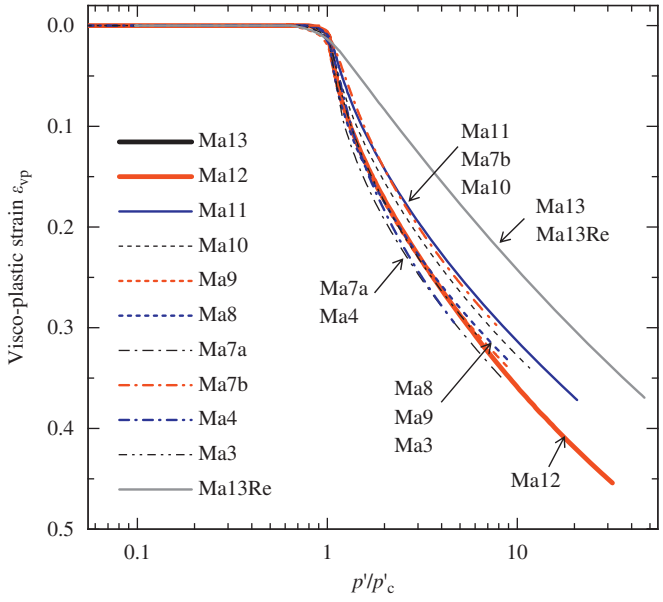

Fig. 3. Superimposed reference compression curves for the Osaka Bay clays.

Consolidation yield stress p'_c is obtained as a function of $\dot{\varepsilon}_{vp}$ from the reference compression curve (ε_{vp}–log ($p'/p'_c(\dot{\varepsilon}_{vp})$)) by using the data set of p' and ε_{vp} (Fig. 5). The method is illustrated in Fig. 6, and the relationships obtained for the clays (Ma10, Ma9, Ma7b, and Ma3) are plotted in Fig. 7. Isotache parameters p'_{cL}, c_1, and c_2 in Eq. (4) are adjusted by fitting them to this log p'_c–log $\dot{\varepsilon}_{vp}$ relationship. The fitting is performed by the least squares method for c_1 and c_2 for various p'_{cL} values. The vertical axis, representing p'_c for the fitting curve, is normalized by p'_{c0}. Here, p'_{c0} is defined as the p'_c corresponding to an $\dot{\varepsilon}_{vp}$ value of $1.0\times10^{-7}\,s^{-1}$.

In Watabe et al. (2008), the consolidation yield stress corresponding to a $\dot{\varepsilon}_{vp}$ value of $3.3\times10^{-6}\,s^{-1}$, which is the strain rate in the CRS tests, was denoted as p'_{c0}. In the present study, however, the consolidation yield stress corresponding to a $\dot{\varepsilon}_{vp}$ value of $1.0\times10^{-7}\,s^{-1}$, which is close to the average strain rate corresponding to the 24-h incremental loading consolidation tests, is denoted as p'_{c0} (Leroueil et al., 1988). This strain rate value was obtained for the series of 24-h incremental loading oedometer tests in practice for the Kansai International Airport project. It is also consistent with the data for Canadian clays shown in Leroueil (2006). We believe that this modification makes its definition much clearer in terms of the essential meaning of p'_{c0} in engineering practice.

For all the depths of the Osaka Bay clays, Watabe et al. (2008) concluded that $p'_{cL}/p'_{c0}=0.55$ can be commonly

Table 2
LT test conditions for the Osaka Bay clays.

Sample	Pressures for preliminary consolidation (kPa)		Pressures for long-term consolidation (kPa)
	24 h (or 2 h) incremental loading	24 h (or 7 days) loading at σ'_{v0}	
Ma13	10→29→	88 (7 days)→	98, 137, 206, 235, 353 and 412
Ma12	39→79→157→	294 (7 days)→	333, 373, 412, 451, 490, 529, 608, 686, 882 and 1370
Ma11	39 (2 h)→	628→	647, 667, 686, 706, 726, 745, 1000 and 1569
Ma10	157→314→627→	1014→	2275 and 2903
Ma9	157→314→627→	1262→	2511 and 3295
Ma8	39 (2 h)→	1373→	1412, 1471, 1530, 1589, 1648, 1726, 1785 and 2040
Ma7a	39 (2 h)→	1491→	1549, 1608, 1667, 1726, 1785, 1844, 1922 and 2177
Ma7b	157→314→627→1255→	1843→	2991
Ma4	39 (2 h)→	1863→	1902, 1961, 2059, 2157, 2256, 2354, 2452 and 3138
Ma3	157→314→627→1255→	2275→	4521
Ma13Re	10→29→	88→	118, 137, 206, 275, 343 and 412

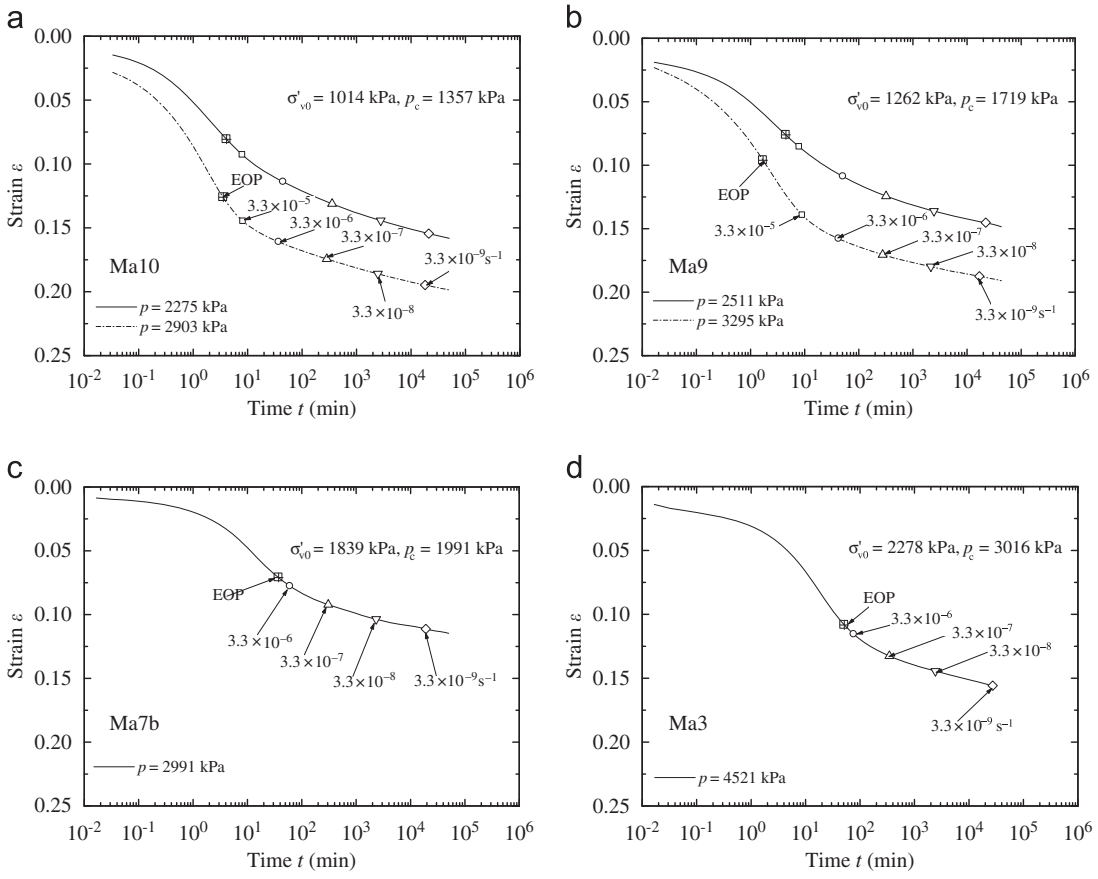

Fig. 4. Consolidation curves (ε–log t curves) observed in the LT tests: (a) Ma10, (b) Ma9, (c) Ma7b and (d) Ma3.

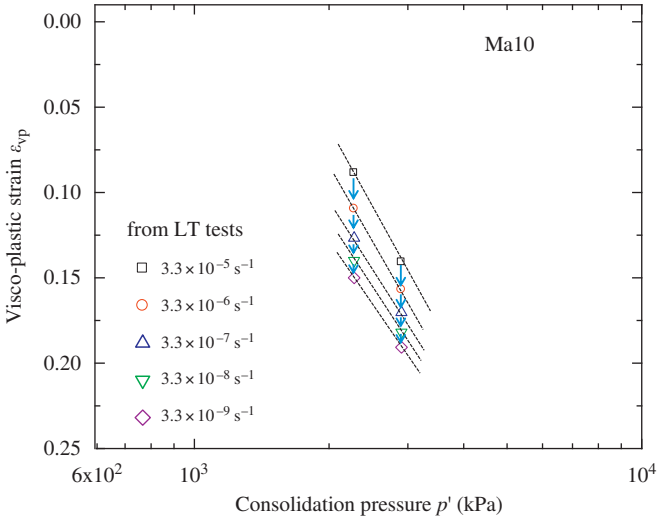

Fig. 5. Strain-rate dependency in ε_{vp}–log p' relationship obtained from the LT tests for Ma10.

used, and then, the other parameters, c_1 and c_2, were also commonly determined as 1.08 and 0.101, respectively. Note here that $p'_{cL}/p'_{c0}=0.55$ with p'_{c0} corresponding to $\dot{\varepsilon}_{vp}=3.3\times10^{-6}\,s^{-1}$ in Watabe et al. (2008) can be converted to $p'_{cL}/p'_{c0}=0.70$ with p'_{c0} corresponding to $\dot{\varepsilon}_{vp}=1.0\times10^{-7}\,s^{-1}$ in the present study. The log p'_c/p'_{c0}–log $\dot{\varepsilon}_{vp}$ relationship evaluated with Eq. (4) is indicated by a solid line in Fig. 7. The isotache parameters were evaluated as, e.g., $p'_{cL}=907.0$ (p'_{cL}/p'_0 was assumed to be 0.70), $c_1=1.05$, and $c_2=0.114$ for Ma10. From the definition, the curve passes through $p'_c/p'_{c0}=1$ at $\dot{\varepsilon}_{vp}=1.0\times10^{-7}\,s^{-1}$. The fitting curve and the test results are compared thoroughly.

When we use $p'_{cL}/p'_{c0}=0.70$ as the common value for all the Osaka Bay clays examined, as concluded by Watabe et al. (2008), isotache parameters p'_{cL}, c_1, and c_2 are determined by the least squares method. Note here that if $p'_c=p'_{c0}$ and $\dot{\varepsilon}_{vp}=1.0\times10^{-7}\,s^{-1}$ are substituted into Eq. (4), parameter c_2 can be expressed as a function of parameter c_1, as follows:

$$c_2=\frac{\ln((p'_c-p'_{cL}/)p'_{cL})-c_1}{\ln\dot{\varepsilon}_{vp}}=\frac{\ln((1-0.7)/0.7)-c_1}{\ln 1.0\times10^{-7}}=\frac{c_1+0.847}{16.12} \tag{5}$$

Then, the following equation is obtained by substituting Eq. (5) into Eq. (4):

$$\ln\frac{p'_c-p'_{cL}}{p'_{cL}}=(1+0.0620\ln\dot{\varepsilon}_{vp})c_1+0.0526\ln\dot{\varepsilon}_{vp} \tag{6}$$

Therefore, the strain-rate dependency of the consolidation yield stress can be essentially expressed with two

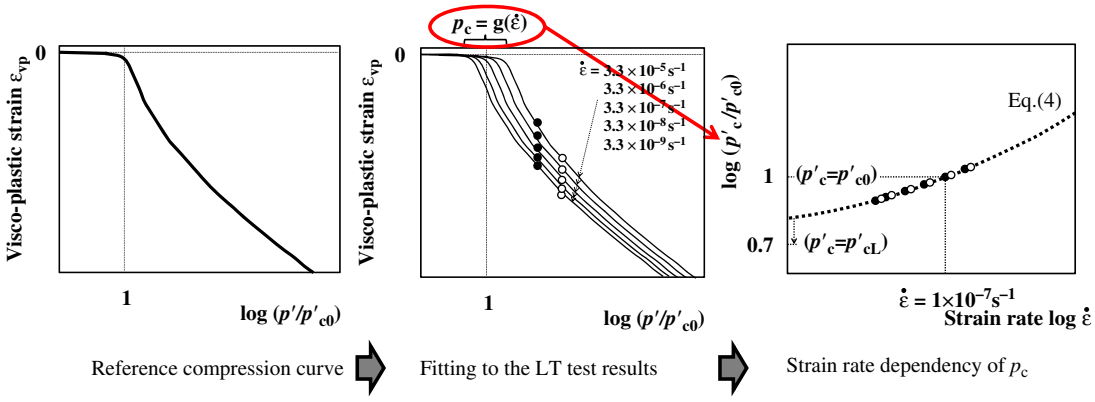

Fig. 6. Illustration of the method to evaluate the strain-rate dependency of p_c from the CRS and the LT test results.

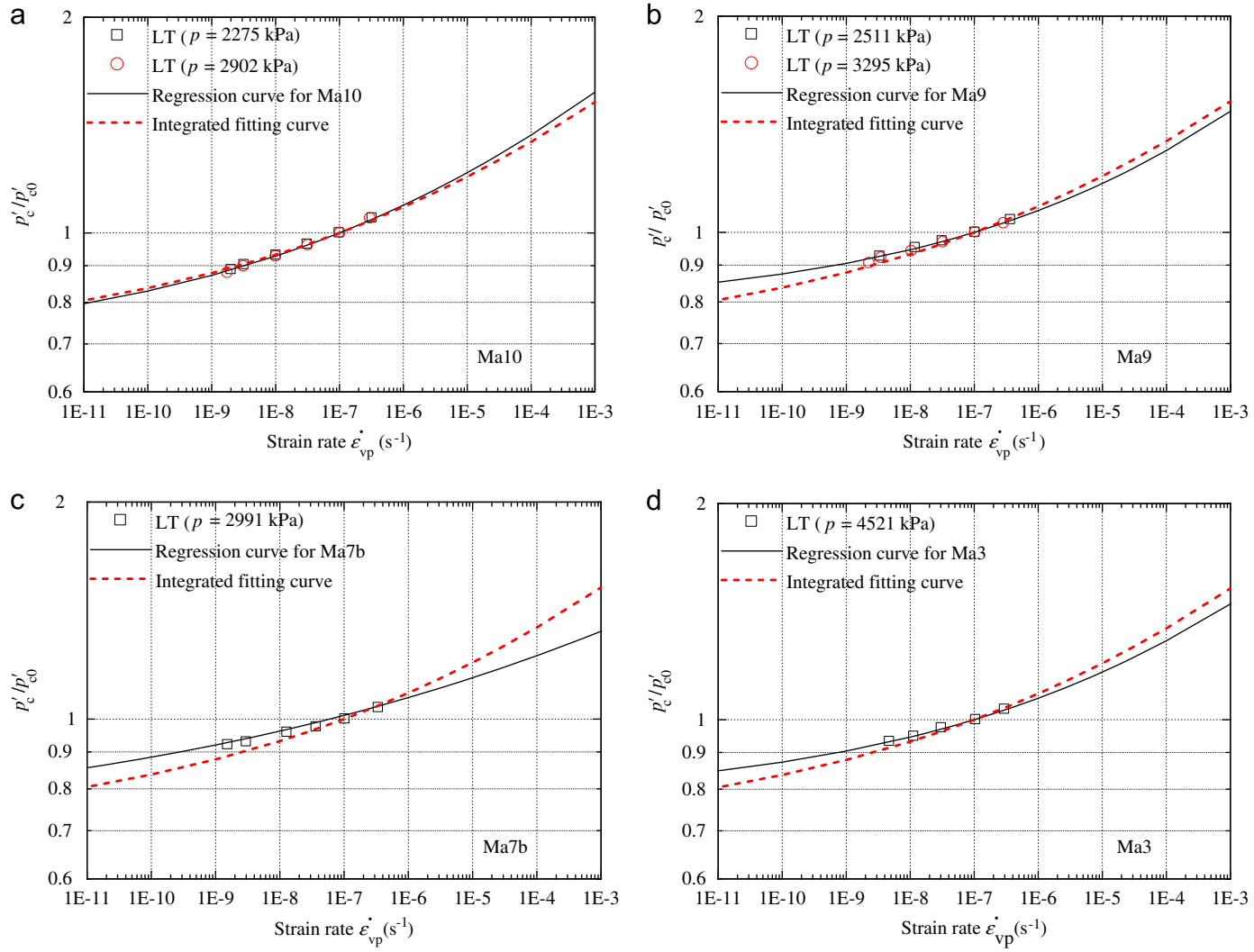

Fig. 7. Log p'_c/p'_{c0}–log $\dot{\varepsilon}_{vp}$ relationships and the fitting with Eq. (4): (a) Ma10, (b) Ma9, (c) Ma7b and (d) Ma3.

isotache parameters, p'_{cL} and c_1, and the other parameter, c_2, is automatically deduced by Eq. (5).

The authors decided to use all the data sets to determine the common isotache parameters, even though the variation in data is larger because the materials examined are natural clays. Consequently, $p'_{cL}/p'_{c0}=0.70$ and $c_1=0.935$ are determined as the common isotache parameters for Osaka Bay clays in this study. The fitting curve

corresponding to $p'_{cL}/p'_{c0}=0.70$ with parameter(s) $c_1=0.935$ (and $c_2=0.107$) is shown by the dotted line in Fig. 7. This fitting curve with the common isotache parameters agrees well with all the test results, indicating that this curve is useful as a primary approximation.

The $\log p'_c/p'_{c0}$–$\log \dot{\varepsilon}_{vp}$ relationship for all the Osaka Bay clays is superimposed in Fig. 8 (including the data shown in Watabe et al. (2008)) comparing it to the fitting curve expressed by Eq. (4) along with the common isotache parameters ($p'_{cL}/p'_{c0}=0.70$ and $c_1=0.935$). The test results and fitting curve are thoroughly compared. This fact indicates that the strain-rate dependency can be modeled by this common fitting curve as an integrated interpretation for the Osaka Bay clays.

The reference compression curves of the Holocene clays (intact Ma13 and remolded Ma13Re) were significantly different from those of the Pleistocene clays (Ma12 and deeper ones). However, it is very interesting that the isotache parameters in the normal consolidation range can be commonly determined for all the specimens of the Osaka Bay clays examined in this study.

Using this integrated fitting curve, consolidation yield stress p'_c is determined as a function of $\dot{\varepsilon}_{vp}$. The compression curve (ε_{vp}–$\log p'$ curve) corresponding to any given $\dot{\varepsilon}_{vp}$ is obtained by multiplying p'/p'_c of the reference compression curve by $p'_c(\dot{\varepsilon}_{vp})$ from the integrated fitting curve. The compression curves for Ma10, derived from the test results using this integrated fitting curve corresponding to $\dot{\varepsilon}_{vp}=3.3\times10^{-5}$, 3.3×10^{-6}, 3.3×10^{-7}, 3.3×10^{-8}, and $3.3\times10^{-9}\,s^{-1}$, are shown in Fig. 9. A special CRS test (SpCRS test) was also carried out for three values of strain rate ((a) $3.3\times10^{-6}\,s^{-1}$, (b) $3.3\times10^{-7}\,s^{-1}$, and (c) $3.3\times10^{-8}\,s^{-1}$) at different stages: (a)→(b)→(c)→(b)→(a)→(b)→(c)→(b)→(a). The horizontal axis of this figure is normalized by consolidation yield stress p'_c corresponding to $\dot{\varepsilon}_{vp}=1.0\times10^{-7}\,s^{-1}$ to compare the results in consideration of the variation in the properties

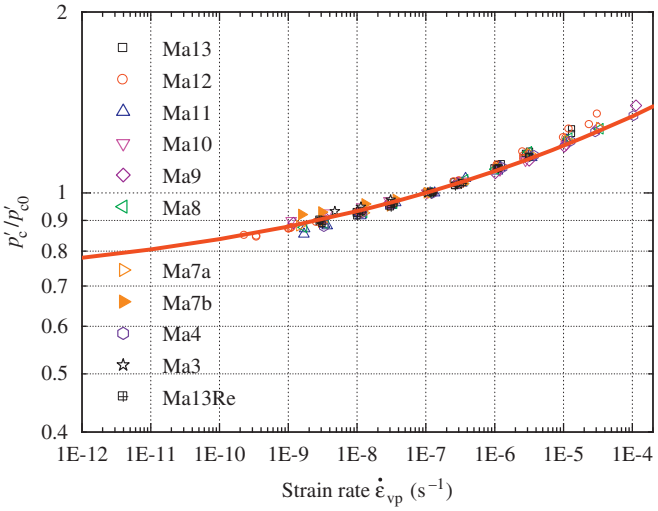

Fig. 8. Log p'_c/p'_{c0}–log $\dot{\varepsilon}_{vp}$ relationship for all the Osaka Bay clays compared to the integrated fitting curve.

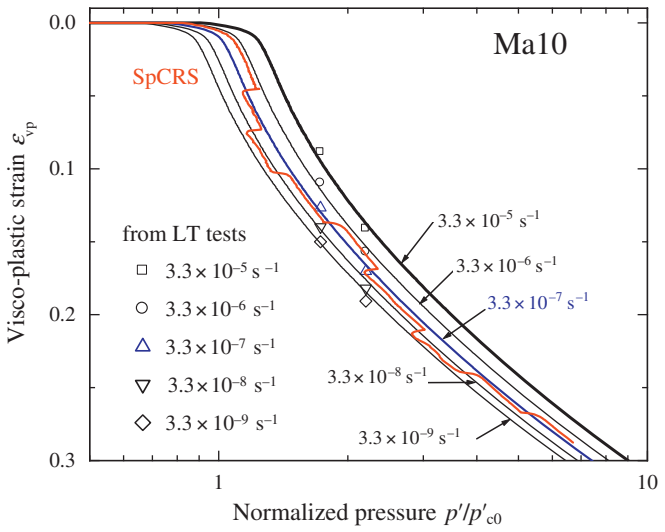

Fig. 9. Compression curves for Ma10 derived from the test results using the integrated fitting curve, compared to the SpCRS test results. The horizontal axis is normalized by consolidation yield stress p'_c corresponding to $\dot{\varepsilon}_{vp}=1.0\times10^{-7}\,s^{-1}$.

of the specimens. The (ε_{vp}, p') data, which are obtained from the secondary consolidation curves in the LT tests (Fig. 5), are also plotted as a function of $\dot{\varepsilon}_{vp}$ in this figure. The compression curves of the integrated curve fitting and the data from the LT tests, as well as the data from the SpCRS test, all fit with the isotache model. Leroueil et al. (1985) observed similar results for the Batiscan clay from the Province of Québec, Canada.

5. Application to worldwide clays

5.1. Comparison to previous data sets—motivation of this study

The integrated fitting curve determined for the Osaka Bay clays in this study and the test results from Leroueil et al. (1988), with an interpretation after Leroueil (2006), are compared in Fig. 10. Here, the parameter representing the vertical axis was obtained as $p'(\dot{\varepsilon})$ at $\varepsilon=10\%$ normalized by $p'(\dot{\varepsilon}=1.0\times10^{-7}\,s^{-1})$ at $\varepsilon=10\%$. There are data from sublayers under well-documented test embankments from Canada and Sweden, and from a variety of laboratory tests. The integrated fitting curve for the Osaka Bay clays is very consistent with the data sets from both laboratory tests and *in situ* observations for the Canadian and Swedish clays. This fact indicates that the integrated fitting curve determined for the Osaka Bay clays should be valid for worldwide clays. In the following part, the applicability of the proposed method to worldwide clays with various characteristics is studied.

5.2. Clay samples

An attempt is made to apply the isotache concept with the integrated fitting curve, determined for the Osaka Bay

clays, to worldwide clays with various characteristics. Nine different clays have been considered in the present study; their physical properties are listed in Table 3.

The Amagasaki clay, Osaka Prefecture, Japan, and the Rakusai clay, Kyoto Prefecture, Japan, are in the family of Osaka Bay clays; however, these clays are characterized by overconsolidation caused by ground uplift. The characteristics of these clays are described by Tanaka et al. (2002). The Ariake clay, Saga Prefecture, Japan, is very sensitive soft clay with a significantly high void ratio. The characteristics of this clay are described in, e.g., Hanzawa et al. (1990). The Haneda clay, Tokyo Metropolitan, Japan, is classified into two groups; i.e., upper clay with high plasticity and lower clay with low plasticity. This clay was sampled during a site investigation of the D-runway construction project at Tokyo's Haneda Airport. The characteristics of this clay are described in Watabe and Noguchi (2011). The Louiseville clay, eastern Canada, is very sensitive clay with a significant cementation effect and mechanical overconsolidation. The main component of the clay particles is glacial rock flour mainly consisting of fine quartz. The characteristics of this clay are described by Leroueil et al. (2003). The Pisa clay, Italy, was sampled in front of the Leaning Tower of Pisa. Its characteristics in void ratio and compression index are similar to those of the Osaka Bay clays. The characteristics of this clay are described in Lo Presti et al. (2003). The Onsøy clay, Norway, is very homogeneous clay with fine particles mainly consisting of glacial rock flour. The characteristics of this clay are described in Lunne et al. (2003). The Mexico City clay, Mexico, is structured clay with very high water content. This is lacustrine clay from a volcanic area. The cementation effect is significant. The characteristics of this clay are described in Díaz-Rodríguez (2003).

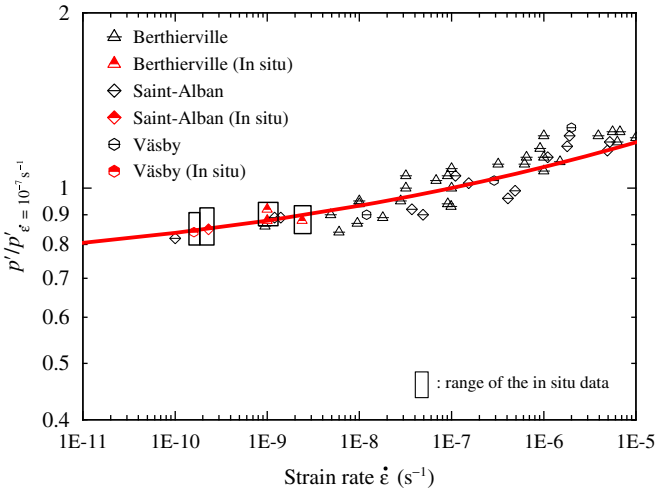

Fig. 10. Normalized stress–strain rate relationship for Canadian and Swedish clays (from Leroueil et al. (1988) with an interpretation after Leroueil (2006)) compared to the integrated fitting curve for the Osaka Bay clays.

5.3. Test results

Both CRS and LT tests were newly conducted for the worldwide clays. The testing procedures are the same as that conducted for the Osaka Bay clays. The test conditions for the LT tests are listed in Table 4. The results obtained from these tests are described below.

The reference compression curves of the nine clays are shown in Fig. 11, in the same manner as Fig. 3 for the Osaka Bay clays. The curve for the Lower Haneda clay shows a bi-linear relationship pattern with the smallest change in visco-plastic strain. These facts are associated with non-structured and low plastic clay. The curves for the other clays exhibit an overshooting around p'_c and a concave shape in the normal consolidation range. This is a typical pattern for structured clays as previously mentioned for the Pleistocene Osaka Bay clays. This tendency is the most significant in the Louiseville clay, which shows a slight decrease in effective vertical stress due to the excess pore water pressure generated by brittle yielding. The curve for the Mexico City clay shows the most significant change in visco-plastic strain due to the high void ratio.

The consolidation curves (ε–log t curves) for the clays obtained from the LT tests are shown in Fig. 12, in the

Table 3
Physical properties of the worldwide clay samples examined in the present study.

Sample	Amagasaki	Rakusai	Ariake	Upper Haneda	Lower Haneda	Louiseville	Pisa	Onsøy	Mexico City
Undisturbed	Yes	Yes	Yes	Yes	Yes	Yes	Yes	Yes	Yes
Reconstituted	No	No	No	No	No	No	No	No	No
Depth (G.L.–m)	34	24	10	10	24	9	17	17	7
Overburden effective stress, σ'_{v0} (kPa)	257	205	51	35	127	62	173	106	26
Consolidation yield stress, p'_c (kPa)	542	846	57	72	242	190	261	129	43
Overconsolidation ratio, OCR	2.1	4.1	1.1	2.1	1.9	3.1	1.5	1.2	1.7
Soil particle density, ρ_s (g/cm^3)	2.69	2.73	2.63	2.69	2.66	2.75	2.76	2.77	2.65
Liquid limit, w_L (%)	124	108	107	153	46	79	99	80	415
Plastic limit, w_P (%)	44	34	45	63	22	22	33	25	64
Plasticity index, I_p	80	74	62	90	24	57	66	55	351
Natural water content, w_n (%)	83	63	139	151	41	74	55	61	395
Natural void ratio, e_n	2.2	1.7	3.7	4.1	1.1	2.0	1.5	1.7	10.5

Table 4
LT test conditions for the worldwide clay samples examined in this study.

Sample	Pressures for preliminary consolidation (kPa)		Pressures for long-term consolidation (kPa)
	24 h (or 2 h) incremental loading	7 days (or 24 h) loading at σ'_{v0}	
Amagasaki	39 (2 h)→	255 (24 h)→	314, 373, 412, 451, 490 and 608
Rakusai	39 (2 h)→	196 (24 h)→	314, 471, 549, 628, 726, 824 and 941
Ariake	9.8→20→	49→	83, 113 and 172
Upper Haneda	4.9→9.8→20→	35→	93 and 152
Lower Haneda	20→39→	127→	314 and 549
Louiseville	10→29→	59→	137, 196, 275, 373 and 471
Pisa	39→78→	176 (24 h)→	177, 265 and 530
Onsøy	20→49→	98→	118, 137, 176, 235 and 353
Mexico City	10→20→	29→	69 and 88

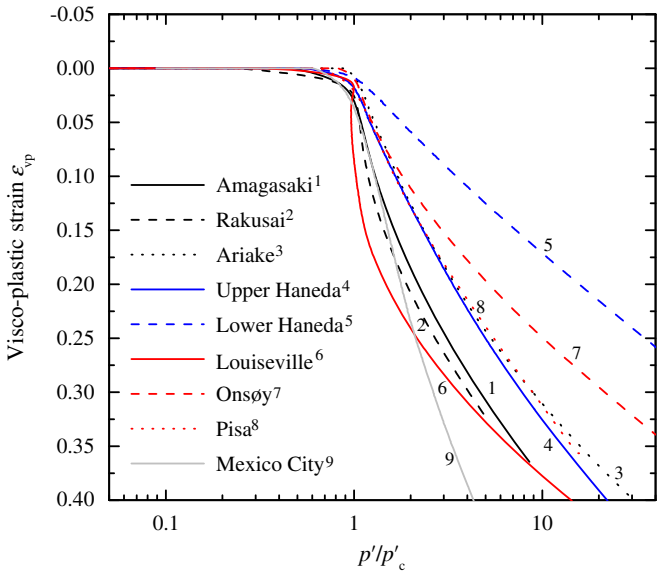

Fig. 11. Superimposed reference compression curves for the worldwide clay samples examined in the present study.

same manner as in Fig. 4 for the Osaka Bay clays. In the normal consolidation range for all the clays, secondary consolidation clearly appears after the EOP. The tendency seen in these curves is very similar to that seen in the curves obtained for the Osaka Bay clays. The points corresponding to the $\dot{\varepsilon}_{vp}$ of 3.3×10^{-6}, 3.3×10^{-7}, 3.3×10^{-8}, and $3.3\times10^{-9}\,s^{-1}$ are shown on the curves.

In the overconsolidated domain, e.g., $p=726$ kPa for the Rakusai clay and $p=137$ kPa for the Louiseville clay, a significant delayed settlement was observed during the secondary consolidation stage. This tendency is consistent with the results obtained for eastern Canada clays (Leroueil et al., 1985) and Osaka Bay clays (Watabe et al., 2008). This fact can be clearly explained with the isotache concept. As illustrated in Fig. 13, even though the clay was originally in an overconsolidated range at a high strain rate, its state surpasses the yield stress p'_c when the strain rate decreases to a significantly smaller value during the secondary consolidation stage under a constant effective stress p'. It is very interesting to note that, for the Rakusai clay, this tendency is very significant in the case of $p=726$ kPa, which is slightly smaller than p'_c. However, it is not observed for the cases of $p\le628$ kPa, for which p is significantly smaller than p'_c.

The values for ε_{vp} corresponding to the $\dot{\varepsilon}_{vp}$ values of 3.3×10^{-6}, 3.3×10^{-7}, 3.3×10^{-8}, and $3.3\times10^{-9}\,s^{-1}$ are obtained from the LT test results. Consolidation yield stress p'_c is obtained as a function of $\dot{\varepsilon}_{vp}$ from the reference compression curve by using the data set of p' and ε_{vp}. The results are plotted in Fig. 14, which corresponds to Fig. 7 for the Osaka Bay clays. Vertical axis p'_c is normalized by p'_{c0}; consequently, all the test results pass through $p'_c/p'_{c0}=1$ at $\dot{\varepsilon}_{vp}=1.0\times10^{-7}\,s^{-1}$. In these figures, the integrated fitting curve with the common isotache parameters determined for the Osaka Bay clays ($p'_{cL}/p'_{c0}=0.70$ and $c_1=0.935$) is superimposed. The trend of the test results, except for the Pisa clay, and the integrated fitting curve are compared thoroughly. Note here that because the results are for natural clays, some variability is inevitable. However, the integrated fitting curve is useful as a primary approximation to conduct a rough calculation for the secondary consolidation behavior, because the difference is not so significant. The model also matches the laboratory results (Fig. 10) obtained by Leroueil et al. (1985), indicating that the model is very general for inorganic clays.

6. Discussion

The reciprocal of p'_{cL}/p'_{c0} seems to be an overconsolidation ratio OCR. The concept of an OCR, at which there is no secondary consolidation, was proposed and demonstrated by Feijo and Martins (1993). The ratio of 0.7 in comparison with the $1.0\times10^{-7}\,s^{-1}$ curve corresponds to OCR=1.43, still with reference to the $1.0\times10^{-7}\,s^{-1}$ strain rate. On the basis of long-term creep tests on the organic Brazilian Sarapui clay, Feijo and Martins (1993) developed the concept of a "zone of indifferent equilibrium" in which there is no significant secondary compression or secondary swelling. In comparison to the end-of-

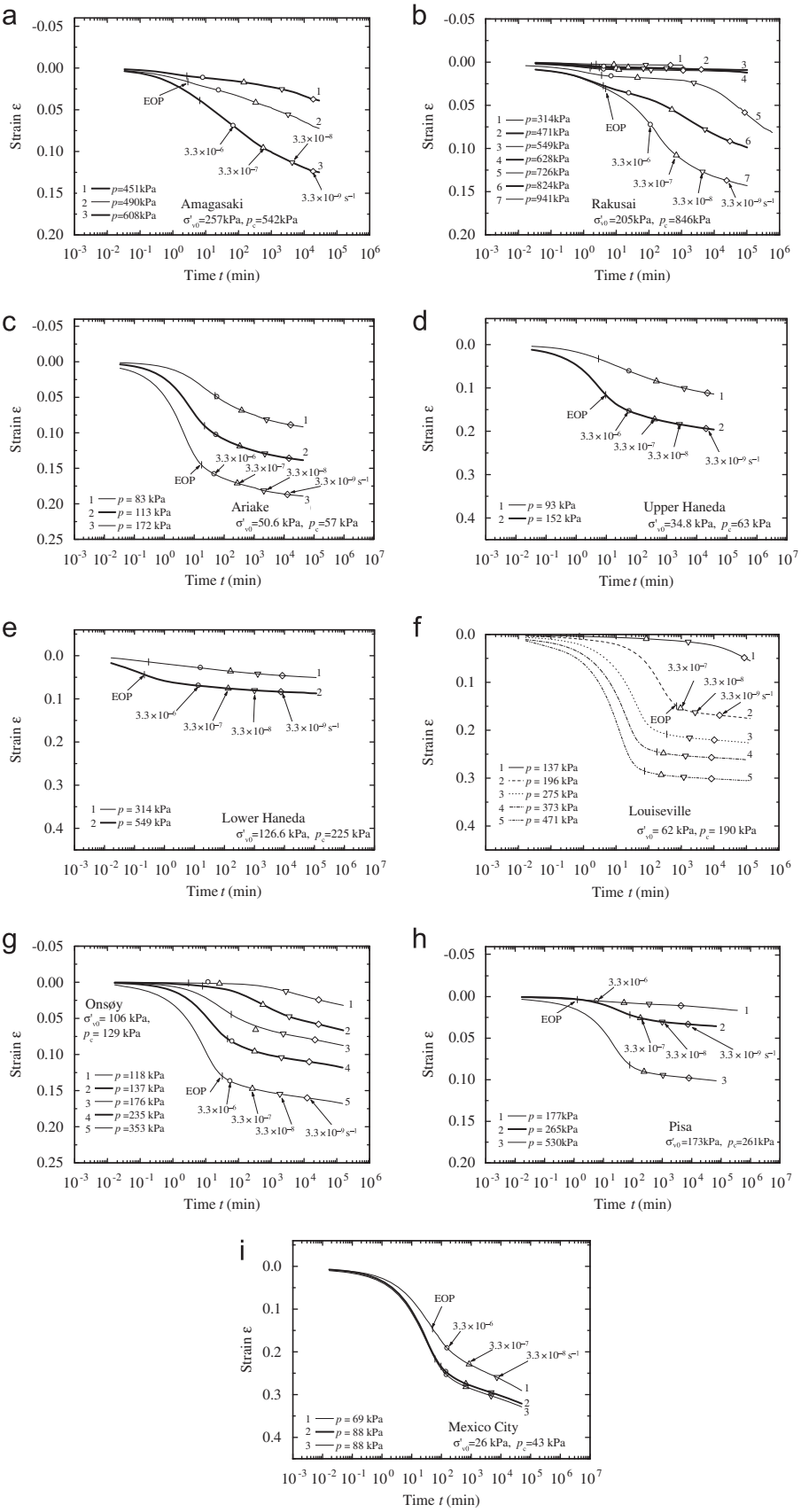

Fig. 12. Consolidation curves (ε–log t curves) observed in the LT tests: (a) Amagasaki clay, (b) Rakusai clay, (c) Ariake clay, (d) Upper Haneda clay, (e) Lower Haneda clay, (f) Louiseville clay, (g) Onsøy clay, (h) Pisa clay and (i) Mexico City clay.

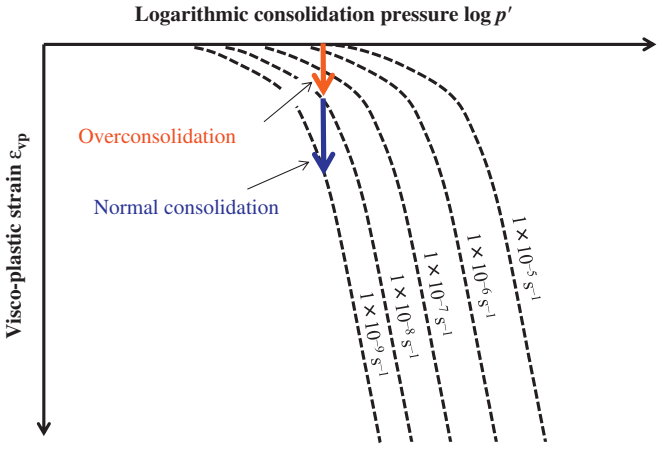

Fig. 13. Illustration of transition from overconsolidation, with a high strain rate, to normal consolidation, with a low strain rate.

primary compression curve, they considered that the minimum OCR at which there was no secondary compression was about 2.0. However, the strain rate at the EOP in Sarapui clays is larger than $1.0\times10^{-6}\,s^{-1}$, and thus, an OCR for that clay in comparison with a curve at a strain rate of $1.0\times10^{-7}\,s^{-1}$ would be smaller than 2 (Martins, personal communication, 2011), but probably larger than 1.43. This could be due to the fact that Sarapui clay is organic. Note here that the clays considered in this study are essentially inorganic.

The test results obtained from the series of LT tests with interpretation along with the reference compression curve (CRS test results) for all the worldwide clays examined, including the Osaka Bay clays (Kansai International Airport Phase 2), as well as the Canadian (Berthierville, Saint-Alban) and Swedish (Väsby) clays (from Leroueil et al. (1988) with an interpretation after Leroueil (2006)), are superimposed in Fig. 15. The integrated fitting curve determined for the Osaka Bay clays is also superimposed in this figure. In addition, *in situ* strain rates and normalized vertical effective stresses obtained under Kansai International Airport Phase 1 have been plotted in Fig. 15. These *in situ* strain rates were calculated from the settlement of sublayers in Ma12 and Ma11 (Furudoi 2010) and its thickness (see Fig. 2). Here, the *in situ* p' was obtained from the applied reclamation pressure, overburden effective stress, and measured excess pore water pressure Δu. For Ma11, the parameter representing the vertical axis for the *in situ* data was obtained as p' ($\dot{\varepsilon}$) at a strain $\varepsilon = 5\%$ normalized with respect to p' ($\dot{\varepsilon} = 1.0\times10^{-7}\,s^{-1}$) at $\varepsilon = 5\%$. For Ma12, however, the p' values obtained from the field observation are normalized with respect to the p' values corresponding to $\dot{\varepsilon}_{vp}=1.0\times10^{-7}\,s^{-1}$ which is obtained from 24-h incremental loading oedometer tests (see Fig. 16), because *in situ* strain was smaller than 5%. Note here that CRS tests were not conducted in the first phase project. It can be seen that the results from the sublayers Ma12 and Ma11 are above and below the integrated fitting curve, respectively. Even if it is considered that uncertainty exists in the results, it can still be concluded, however, that this observation is consistent with the field and the laboratory data obtained for clays from eastern Canada and Sweden (Fig. 10) by Leroueil et al. (1988).

The compression curves observed for Ma12 under Kansai International Airport Phase 1, together with the isotache model deduced from the 24-h incremental loading oedometer tests with the integrated fitting curve, are shown in Fig. 16. The oedometer tests were performed on samples taken at a different location from the site of the sublayer measurements under Kansai International Airport Phase 1. Here, the reference compression curve is the average of 5 test results at different depths at 2-m intervals. It can be seen that the two sets of data do not fit perfectly; effective stresses of the first set are larger than those of the second set for the same strain and strain rate. However, the data shows that the slope of the *in situ* compression curve associated with decreasing strain rates is much steeper than the slope of the isotaches, in agreement the isotache model. It confirms that clays in the laboratory and *in situ* are influenced in the same way by the strain rate and follow the same constitutive model.

It is very interesting to observe that the integrated fitting curve with the common isotache parameters, initially determined for the Osaka Bay clays, can be applicable to the worldwide essentially inorganic clays with various characteristics, even for the Mexico City clay whose characteristics are very exceptional compared to more usual clays, e.g., with very high water content w (or void ratio e) and a cemented structure.

Since the integrated fitting curve is widely applicable, it is not necessary, in practice, to carry out LT tests that require very long testing periods. Actually, the range of $\dot{\varepsilon}_{vp}$ obtained from the LT tests is generally limited to the range of 10^{-9} to $10^{-5}\,s^{-1}$; however, the strain rates observed *in situ* can be much smaller than this. If we have a reference compression curve, which can be easily obtained from CRS tests, the viscous behavior can be estimated by considering the strain-rate dependency, i.e., the isotache concept, represented by the integrated fitting curve.

The slope of the $\log(p'_c/p'_{c0})$–$\log\dot{\varepsilon}_{vp}$ relationship at a given strain rate (denoted as α) corresponds to the ratio of secondary compression index $C_{\alpha e}$ to the compression index C_c, expressed as

$$\alpha=\frac{\Delta\log(p'_c/p'_{c0})}{\Delta\log\dot{\varepsilon}_{vp}}=\frac{\Delta\log p'_c}{\Delta\log\dot{\varepsilon}_{vp}}=\frac{C_{\alpha e}}{C_c} \tag{7}$$

Mesri and Castro (1987) proposed a practical concept in which $C_{\alpha e}/C_c$ would be constant. For inorganic clays, this ratio is typically equal to 0.04 ± 0.01 (Mesri et al., 1995). Fig. 17 shows (a) a comparison of the integrated fitting curve with the constant $C_{\alpha e}/C_c$ concept with $\alpha=0.04$ and (b) the relationship between α and the strain rate calculated from the integrated fitting curve. As seen in Fig. 17(b), $\alpha=C_{\alpha e}/C_c$ is not a constant and decreases when $\dot{\varepsilon}_{vp}$ decreases. This is consistent with the fact emphasized in Leroueil (2006) with the data for the Canadian and Swedish clays (see Fig. 10) and confirmed in

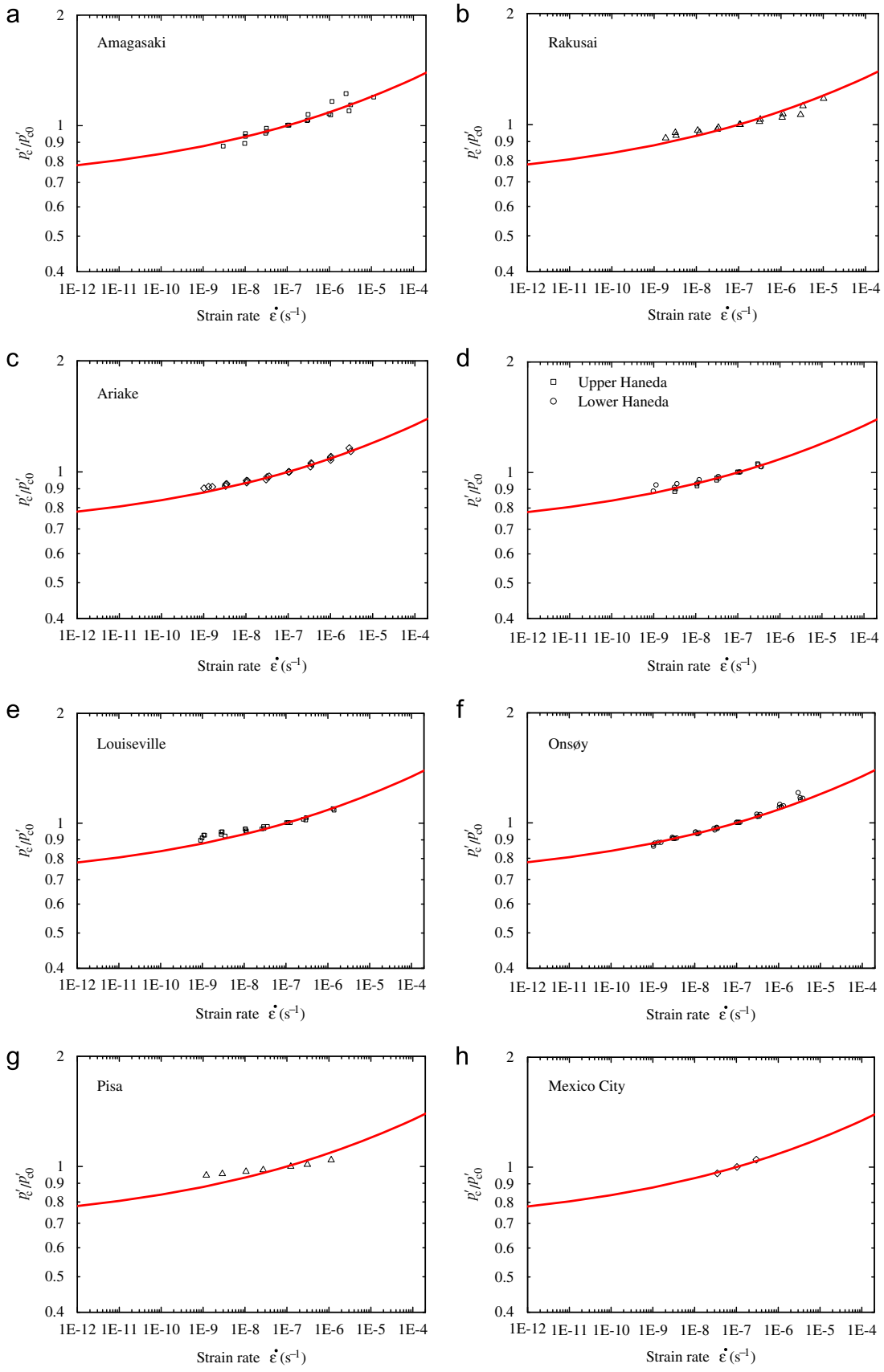

Fig. 14. Log p'_c/p'_{c0}–log $\dot{\varepsilon}_{vp}$ relationships compared to the integrated fitting curve for the Osaka Bay clays: (a) Amagasaki clay, (b) Rakusai clay, (c) Ariake clay, (d) Upper and Lower Haneda clays, (e) Louiseville clay, (f) Onsøy clay, (g) Pisa clay and (h) Mexico City clay.

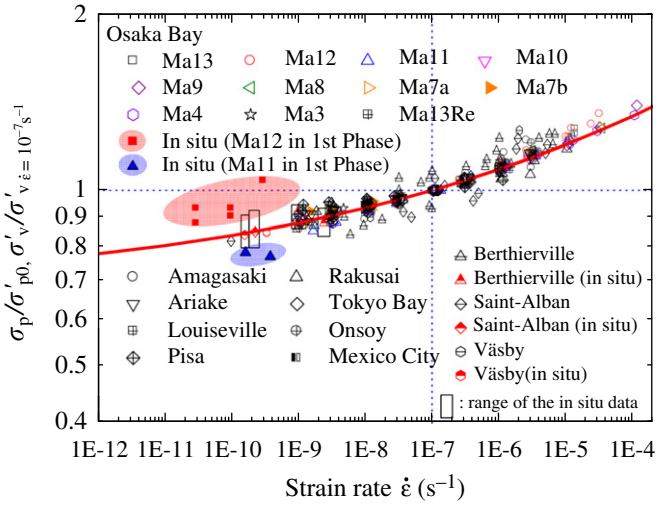

Fig. 15. Log p'_c/p'_{c0}–log $\dot{\varepsilon}_{vp}$ relationship for all the worldwide clays examined, including the Osaka Bay clays, compared to the integrated fitting curve.

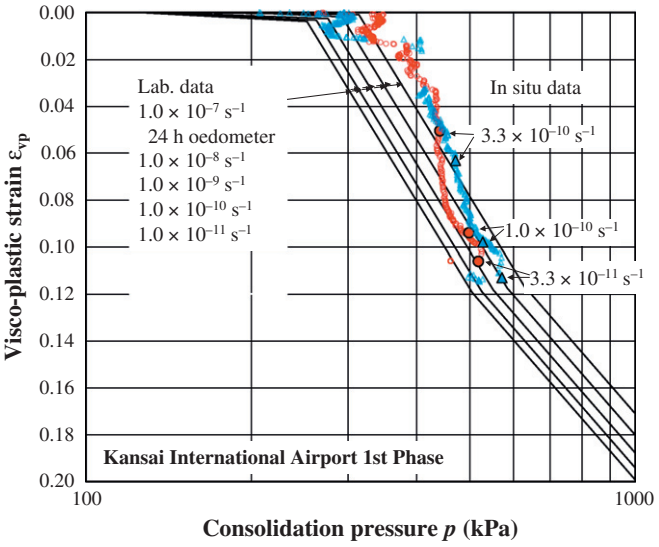

Fig. 16. Compression curves observed for Ma12 under Kansai International Airport Phase 1 together with the isotache model deduced from 24-h incremental loading oedometer tests, corresponding to the strain rates of 1.0×10^{-7} s^{-1}. The oedometer tests were performed on samples taken at a different location from the site of the sublayer measurements under Kansai International Airport Phase 1. Here, the reference compression curve is an average of 5 test results at different depths and at 2-m intervals.

the present paper for the worldwide clays. For the integrated fitting curve, the value of α equals 0.04 at a strain rate of 1×10^{-6} s^{-1}. Then, the value of p'_c/p'_{c0} converges to 0.7 for the integrated fitting curve, with, for example, α being equal to 0.035 and 0.019 at strain rates of 1×10^{-7} s^{-1} and 1×10^{-10} s^{-1}, respectively. This tendency is consistent with the comments in Leroueil (2006) and quantitatively clarified in this study. It appears that $C_{\alpha e}/C_c = 0.04 \pm 0.01$ is essentially valid for strain rates between 1×10^{-5} and 1×10^{-8} s^{-1}, i.e., strain rates generally observed in the laboratory, which explains the observation made by Mesri and his co-workers. The integrated fitting curve (Eq.(4) with the common isotache parameters) is obtained for mostly inorganic clays; however, it would be interesting to, using Eq.(7), define the asymptotic value of p'_c/p'_{c0} to have, $C_{\alpha e}/C_c$ equals to 0.02 (cohesionless soils), 0.05 (organic clays) and 0.06 (peat) (Mesri et al., 1995). Because data for these other classes of materials are not available, this behavior cannot be extrapolated to smaller strain rates, at which clay deposits under embankments generally are.

Fig. 18 schematically illustrates the compression curve which would be obtained from LT tests in the laboratory (A→C→D→E) and *in situ* observations (A→B→E→F) for an incremental loading from the overburden effective stress σ'_{v0} to a vertical pressure p'_1 in the post-yield domain. In the figure, the compression curves corresponding to several strain rates are superimposed. The curve for the infinitesimal strain rate represents the maximum potential compression of the clay. Points D, E, and F correspond to the strain rates of 1.0×10^{-7} s^{-1}, 1.0×10^{-10} s^{-1}, and $1.0 \times 10^{-\infty}$ (infinitesimal strain rate) s^{-1}, respectively. From our experience, the minimum strain rates obtained from the LT tests are generally around 1.0×10^{-9} s^{-1}; therefore, the path cannot reach point E. The strain rates obtained from the *in situ* observations at the Kansai International Airport are currently around 3.3×10^{-11} s^{-1}, corresponding to a primary consolidation stage, and may become smaller than this at the EOP corresponding to the point E. However, the path cannot reach point F.

In engineering practice, consolidation settlement is generally estimated based on the e–log p curve obtained from 24-h incremental loading oedometer tests which corresponds to a strain rate of about 1.0×10^{-7} s^{-1} (point D). Using compression index C_c at consolidation pressure p'_1, the maximum potential additional settlement can be estimated as follows from the geometric relation:

$$\Delta\varepsilon_{D\to F} = \frac{C_c}{1+e_0}\log\frac{p'_{c0}}{p'_{cL}} \tag{8}$$

$$\Delta\varepsilon_{D\to E} = \frac{C_c}{1+e_0}\log\left[\frac{p'_{c0}}{p'_{cL}}\left\{\frac{1}{1+\exp(c_1+c_2\ln\dot{\varepsilon}_{EOP})}\right\}\right] \tag{9}$$

Here $\dot{\varepsilon}_{EOP}$ is the strain rate at the *in situ* end of primary consolidation. Note here that $p'_{cL}/p'_{c0}=0.7$ can be commonly used for the worldwide clays. In the case of Ma12 of the Osaka Bay clays, for example, initial void ratio e_0 and C_c are typically 2.2 (Table 1) and 1.0 (Watabe et al., 2002), respectively, corresponding to a natural water content of around 100%. Consequently, using Eq.(8) $\Delta\varepsilon_{D\to F}$ can be estimated to 0.048 (4.8%). In addition, because an *in situ* strain rate for Ma12 at the Kansai International Airport is typically 3.3×10^{-11} s^{-1}, as evaluated from the settlement of the sublayers, using Eq.(9) (or using Eq.(8) by replacing $p'_{cL}/p'_{c0}=0.7$ by $p'_c(\dot{\varepsilon}_{vp}=1.0 \times 10^{-10}\ s^{-1})/p'_{c0}=0.82$ for the integrated fitting curve (Fig. 15)), $\Delta\varepsilon_{D\to E}$ can be estimated to 0.025 (2.5%); this is roughly what has been observed.

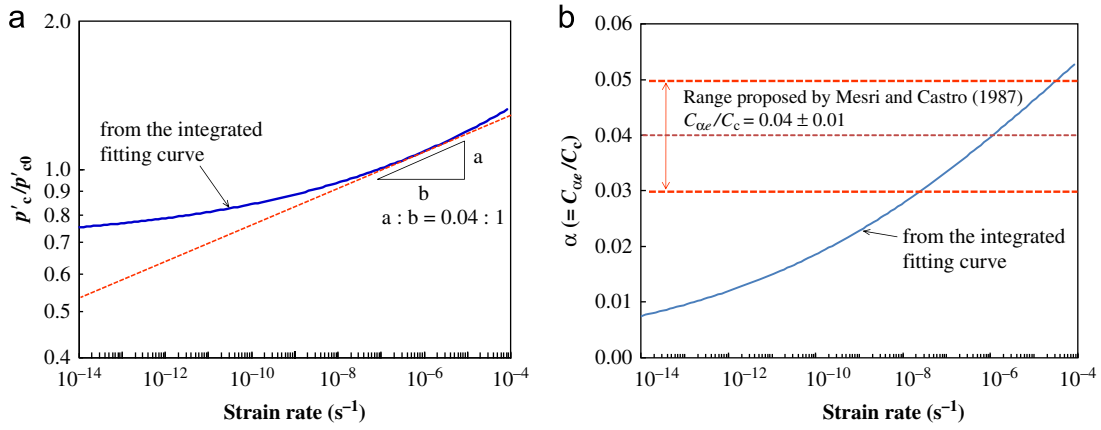

Fig. 17. Comparison of the integrated fitting curve with the constant $C_{\alpha e}/C_c$ concept: (a) relationship between p'_c/p'_{c0} and strain rate and (b) relationship between α ($=C_{\alpha e}/C_c$) and strain rate.

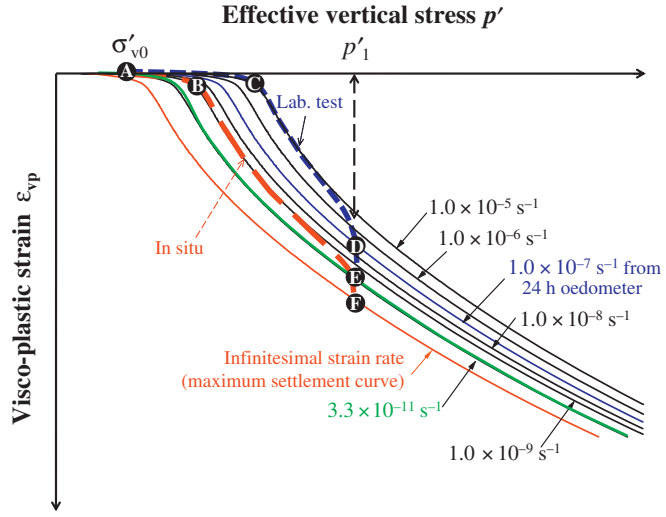

Fig. 18. Schematic illustration of compression paths for LT tests in the laboratory and the *in situ* behavior.

7. Conclusions

Watabe et al. (2008) proposed a simplified method based on the isotache concept by using a compression curve and the relationship between the consolidation yield stress (preconsolidation pressure) and the strain rate. The former and the latter are obtained from constant rate of strain consolidation (CRS) tests and long-term consolidation (LT) tests, respectively. The latter is expressed by Eq. (4) with three isotache parameters (p'_{cL}, c_1, and c_2).

In the present study, additional tests in a series of CRS and LT tests for the clay samples collected at various depths (up to 300 m below the seabed) in Osaka Bay, after Watabe et al. (2008), were carried out to update the data sets of the test results. The isotache parameters are $p'_{cL}/p'_{c0}=0.70$ and $c_1=0.935$ for all the depths of the Osaka Bay clays. Here, p'_{c0} is defined as the consolidation yield stress corresponding to $\dot{\varepsilon}_{vp}=1.0\times10^{-7}\,s^{-1}$, which is close to the average strain rate corresponding to the 24-h incremental loading oedometer tests. This fitting curve is named the integrated fitting curve. Parameter c_2 is calculated by Eq. (5) as a function of parameters p'_{cL}/p'_{c0} and c_1.

A series of CRS tests and LT tests were carried out for worldwide clays with various characteristics in plasticity, minerals, structures, cementations, overconsolidation, etc. and then the proposed method was applied to those test results. It was found that the common isotache parameters determined for the Osaka Bay clays are applicable to all the worldwide clays, even for the Mexico City clay whose characteristics are very exceptional compared to usual soils, with a water content w of almost 400%. The integrated fitting curve for the Osaka Bay clays is very consistent with the data sets of the worldwide clays from both laboratory tests and *in situ* observations. If there is a reference compression curve, which can be easily obtained from CRS tests, the viscous behavior can be estimated in consideration of the strain-rate dependency, i.e., the isotache concept, represented by the integrated fitting curve.

The slope of the $\log(p'_c/p'_{c0})$–$\log\dot{\varepsilon}_{vp}$ relationship at a given strain rate (denoted as α), which corresponds to the ratio of secondary compression index $C_{\alpha e}$ to compression index C_c, can be calculated from the integrated fitting curve, showing that it is not constant, but decreases with $\dot{\varepsilon}_{vp}$. This tendency is consistent with the comments in Leroueil (2006), and is quantitatively clarified in this study.

In engineering practice, the consolidation settlement is generally estimated based on the e–$\log p'$ curve obtained from 24-h incremental loading oedometer tests which corresponds to a strain rate of about $1\times10^{-7}\,s^{-1}$. Using compression index C_c at consolidation pressure p', the maximum potential additional settlement can be estimated by Eq. (8) with $p'_{cL}/p'_{c0}=0.7$, which can be commonly used for the worldwide clays.

Acknowledgments

The study presented in this paper was carried out as a part of the collaborative research between the Port and Airport Research Institute (PARI) and the Kansai International Airport Land Development Co., Ltd. (KALD). We would like to thank Dr. Masaki Kobayashi of the

Coastal Development Institute of Technology (CDIT) for his active discussions on this study.

References

Adachi, T., Oka, F., Mimura, M., 1996. Modeling aspects associated with time dependent behavior of soils. Session on Measuring and Modeling Time Dependent Soil Behavior, ASCE Convention, Washington, Geothnical Special Publication, vol. 61, pp. 61–95.

Degago, S.A., Grimstad, G., Jostad, H.P., Nordal, S., Olsson, M., 2011. Use and misuse of the isotache concept with respect to creep hypotheses A and B. Géotechnique 61 (10), 897–908.

Den Haan, E.J., Kamao, S., 2003. Obtaining isotache parameters from a C.R.S. K_0-oedometer. Soils and Foundations 43 (4), 203–214.

Díaz-Rodríguez, 2003. Characterization and engineering properties of Mexico City lacustrine soils. In: Tan (Ed.), Characterisation and Engineering Properties of Natural Soils. Swets & Zeitlinger, Lisse, pp. 725–755.

Feijo, R.L., Martins, I.M.S., 1993. Relationship between secondary compression, OCR and K_0. COPPEGEO '93, COPPE/Federal University of Rio de Janeiro, pp. 27–40 (in Portuguese).

Furudoi, T., 2010. The second phase construction of Kansai International Airport considering the large and long-term settlement of the clay deposits. Soils and Foundations 50 (6), 805–816.

Hanzawa, H., Fuyaka, T., Suzuki, K., 1990. Evaluation of engineering properties for an Ariake clay. Soils and Foundations 30 (4), 11–24.

Hinchberger, S.D., Rowe, R.K., 1998. Modelling the rate-sensitive characteristics of the Gloucester foundation soil. Canadian Geotechnical Journal. 35 (5), 769–789.

Imai, G., Ohmukai, N., Tanaka, H., 2005. An isotaches-type compression model for predicting long term consolidation of KIA clays. In: Proceedings of the Symposium on Geotechnical Aspects of Kansai International Airport, pp. 49–64.

Kim, Y.T., Leroueil, S., 2001. Modelling the viscoplastic behaviour of clays during consolidation: application to Berthierville clay in both laboratory and field conditions. Canadian Geotechnical Journal 38 (3), 484–497.

Leroueil, S., 2006. The isotache approach. Where are we 50 years after its development by Professor Šuklje? (2006 Prof. Šuklje's Memorial Lecture). In: Proceedings of the 13th Danube-European Conference on Geotechnical Engineering, Ljubljana 2006, pp. 55–88.

Leroueil, S., Kabbaj, M., Tavenas, F., Bouchard, R., 1985. Stress–strain–strain rate relation for the compressibility of sensitive natural clays. Géotechnique **35** (2), 159–180.

Leroueil, S., Kabbaj, M., Tavenas, F., 1988. Study of the validity of a σ'_v–ε_v–ε_v model in in situ conditions. Soils and Foundations 28 (3), 3–25.

Leroueil, S., Hamouche, K., Tavenas, F., Boudali, M., Locat, J., Virely, D., Roy, M., La Rochelle, P., Leblond, P., 2003. Geotechnical characterization and properties of a sensitive clay from Québec. In: Tan (Ed.), Characterisation and Engineering Properties of Natural Soils. Swets & Zeitlinger, Lisse, pp. 363–394.

Lo Presti, D.C.F., Jamiolkowski, M., Pepe, M., 2003. Geotechnical characterisation of the subsoil of Pisa Tower. In: Tan (Ed.), Characterisation and Engineering Properties of Natural Soils. Swets & Zeitlinger, Lisse, pp. 909–946.

Lunne, T., Long, M., Forsberg, C.F., 2003. Characterisation and engineering properties of Onsøy. In: Tan (Ed.), Characterisation and Engineering Properties of Natural Soils. Swets & Zeitlinger, Lisse, pp. 395–427.

Mesri, G., Choi, Y.K., 1985. The uniqueness of the end-of-primary (EOP) void ratio-effective stress relationship. In: Proceedings of the 11th ICSMFE, San Francisco, vol. 2, pp. 587–590.

Mesri, G., Castro, A., 1987. The C_a/C_c concept and K_0 during secondary compression. Journal of Geotechnical Engineering, ASCE 113 (3), 230–247.

Mesri, G., Shahien, M., Feng, T.W., 1995. Compressibility parameters during primary consolidation. In: Proceedings of the International Symposium on Compression and Consolidation of Clayey Soils, IS-Hiroshima 95, Hiroshima, vol. 2, pp. 1021–1037.

Norton, F.H., 1929. The Creep of Steel at High Temperature. McGraw-Hill, New York.

Perzyna, P., 1963. Constitutive equations for rate sensitive plastic materials. Quarterly of Applied Mathematics 20 (4), 321–332.

Qu, G., Hinchberger, S.D., Lo, K.Y., 2010. Evaluation of the viscous behaviour of clay using generalized overstress viscoplastic theory. Géotechnique 60 (10), 777–789.

Rowe, R.K., Hinchberger, S.D., 1998. The significance of rate effects in modelling the Sackville test embankment. Canadian Geotechnical Journal 35 (3), 500–516.

Šuklje, L., 1957. The analysis of the consolidation process by the isotache method. In: Proceedings of the 4th International Conference on Soil Mechanics and Foundation Engineering, London, vol. 1, pp. 200–206.

Tanaka, H., Ritoh, F., Omukai, N., 2002. Quality of samples retrieved from great depth and its influence on consolidation properties. Canadian Geotechnical Journal 39 (6), 1288–1301.

Tanaka, H., Udaka, K., Nosaka, T., 2006. Strain rate dependency of cohesive soils in consolidation settlement. Soils and Foundations 46 (3), 315–322.

Watabe, Y., Tsuchida, T., Adachi, K., 2002. Undrained shear strength of Pleistocene clay in Osaka Bay. Journal of Geotechnical & Geoenvironmental Engineering, ASCE 128 (3), 216–226.

Watabe, Y., Udaka, K., Morikawa, Y., 2008. Strain rate effect on long-term consolidation of Osaka bay clay. Soils and Foundations 48 (4), 495–509.

Watabe, Y., Noguchi, T., 2011. Site-investigation and geotechnical design of D-runway construction in Tokyo Haneda Airport. Soils and Foundations 51 (6), 1003–1018.

Yin, J.H., Graham, J., Clark, J.L., Gao, L., 1994. Modelling unanticipated pore-water pressures in soft clays. Canadian Geotechnical Journal 31 (5), 773–778.